

# Noncovalent solubilization of multi-walled carbon nanotubes in common low-polarity organic solvents with branched Pd–diimine polyethylenes: Effects of polymer chain topology, molecular weight and terminal pyrene group



Lixin Xu <sup>a</sup>, Zhibin Ye <sup>a,\*</sup>, Stefan Siemann <sup>b</sup>, Zhiyong Gu <sup>c</sup>

<sup>a</sup> Bharti School of Engineering, Laurentian University, Sudbury, Ontario P3E 2C6, Canada

<sup>b</sup> Department of Chemistry and Biochemistry, Laurentian University, Sudbury, Ontario P3E 2C6, Canada

<sup>c</sup> Department of Chemical Engineering, University of Massachusetts Lowell, Lowell, MA 01854, USA

## ARTICLE INFO

### Article history:

Received 24 March 2014

Received in revised form

6 May 2014

Accepted 7 May 2014

Available online 20 May 2014

### Keywords:

Multi-walled carbon nanotubes

Hyperbranched polyethylene

Noncovalent nonspecific solubilization

## ABSTRACT

Noncovalent nonspecific solubilization of carbon nanotubes with common polymers without having any specific functionality is an important strategy for rendering debundled nanotube solutions for their processing and technological applications. Among the various polymers investigated thus far for noncovalent nonspecific nanotube solubilization, hyperbranched polyethylene (HBPE) featured with distinct highly compact dendritic chain architecture has been discovered to show outstanding performance in rendering stable nanotube solutions in common low-polarity organic solvents (including tetrahydrofuran (THF) and chloroform) at surprisingly high concentrations. To understand the mechanism of the nanotube solubilization with this unique class of polymers and to elucidate the effects of various macromolecular structural parameters, we have designed and synthesized in this work four sets of highly branched polyethylenes varying in chain topology, molecular weight, and end group. With these polymers, we have systematically investigated and compared their performance for the solubilization of multi-walled carbon nanotubes in common solvents including THF, chloroform, *n*-heptane, and toluene. We have found that these macromolecular structural parameters as well as the solvent play complex but sensitive roles in this noncovalent solubilization system. This work thus provides some valuable guidelines towards the design of optimum polymers for efficient noncovalent nonspecific solubilization of carbon nanotubes.

© 2014 Elsevier Ltd. All rights reserved.

## 1. Introduction

Stable dispersion or solubilization of carbon nanotubes (CNTs) in aqueous or organic solvents at high concentrations has been critically important to the processing and applications of these nanomaterials of outstanding properties in various emerging fields [1–6]. CNTs always tend to aggregate in most solvents, originating from their high aspect ratios and strong van der Waals interactions between these nanomaterials. One of the solutions to this problem is surface functionalization of CNTs with organic polymers, which can impart modified CNTs with required surface functionalities and significantly improved dispersibility in desired solvents [7–10]. So

far, two general strategies, covalent [11,12] and noncovalent [13,14], have been extensively explored for surface functionalization of CNTs with polymers [7–10]. Through the covalent strategy, numerous polymers have been covalently grafted onto nanotube surface via two different methodologies, including “grafting-from” surface-initiated living/controlled polymerization techniques and “grafting-to” reaction of tailor-made reactive polymers with functional groups on nanotube surface [11,12]. Though efficient in rendering soluble CNTs, this covalent functionalization strategy inevitably leads to considerable disruption in the  $\pi$ -orbital structure of CNTs and thus their compromised properties.

In the noncovalent strategy, CNTs are surface functionalized with polymers by noncovalent sidewall adsorption or wrapping through either specific or nonspecific interactions between the polymers and nanotube sidewalls [7–10,13,14]. This strategy has the advantage of preserving the structural integrity of CNTs and

\* Corresponding author. Fax: +1 705 675 4862.

E-mail address: [zye@laurentian.ca](mailto:zye@laurentian.ca) (Z. Ye).

consequently their uncompromised properties, and is thus preferred. In the case of noncovalent specific functionalization, numerous specially designed polymers bearing various specific functionalities are used to establish noncovalent specific interactions, such as  $\pi$ – $\pi$  stacking with the use of conjugated polymers [15–24] or pyrene-containing polymers [25–32], ionic interactions with the use of polyelectrolytes [33–37], etc., between the polymers and nanotube sidewalls. Synthesis of these specialty polymers, however, often involves the use of specially designed functional monomers/molecules and/or sophisticated polymerization techniques, which is unfavorable for the large-scale industrial applications of CNTs [38]. The noncovalent nonspecific functionalization, on the other hand, often employs the nonspecific CH– $\pi$  interactions between nanotube sidewalls and conventional polymers without any specific functionalities. Given the need of only conventional polymers made from common abundant monomer stocks, this noncovalent nonspecific approach is particularly desired for the solubilization of CNTs.

Baskaran et al. were the first to report the noncovalent nonspecific solubilization of multiwalled carbon nanotubes (MWCNTs) with the use of conventional polymers, including polybutadiene, polyisoprene, polystyrene, and polymethylmethacrylate, via CH– $\pi$  interactions [39]. They have suggested that the polymer adsorption or wrapping around CNTs is a general phenomenon. However, the solubility of MWCNTs in organic solvents (such as  $\text{CHCl}_3$ ) achieved in their study is too low (below 0.020 mg/mL) for practical applications, possibly due to the weakness of CH– $\pi$  interactions. In addition, some other conventional nonfunctionalized polymers, including poly(*N*-isopropylacrylamide) [40], poly(acrylic acid) [41], poly(dialkylsilane) [42], and poly(*N*-(2-(dimethylamino)ethyl)methacrylate) [43], were also demonstrated to functionalize and disperse CNTs in organic solvents via CH– $\pi$  interactions. Though effective nanotube dispersions were obtained in these latter cases, the nanotube solubility data, presumably low, were not disclosed. Superior to these reported polymers in terms of nanotube solubility, our group demonstrated in 2009 the use of a hyperbranched polyethylene (HBPE) for the noncovalent nonspecific functionalization and solubilization of MWCNTs in organic solvents (tetrahydrofuran, THF, and chloroform), which rendered strikingly high nanotube concentrations (up to ca. 1235 mg/L in chloroform and 920 mg/L in THF) [38]. These nanotube solubility data achieved with HBPE are comparable to or even greater than the highest values ever achieved in organic solvents in the literature with the use of special conjugating polymers capable of forming  $\pi$ – $\pi$  interactions with nanotube sidewalls [23]. HBPE is a new grade of polyethylene synthesized directly and solely from ethylene through the well-known Pd–Diimine-catalyzed chain walking polymerization [44,45]. The adsorption of HBPE on nanotube sidewalls has been observed with transmission electron microscopy (TEM) [38]. In subsequent studies [46,47], HBPE-functionalized MWCNTs were also shown to have significantly enhanced dispersion in ethylene–octene copolymer due to the presence of HBPE around the nanotubes, which dramatically improves the compatibility of the nanotubes with the matrix polymer. Recently, we have further discovered that HBPE also efficiently facilitates the production of stable dispersions of high-quality few-layer graphene sheets at high concentrations in THF and chloroform through ultrasonication-assisted liquid-phase exfoliation of graphite [48]. Similarly, HBPE was found to adsorb on the surface of exfoliated graphene sheets through CH– $\pi$  interactions, preventing their restacking and rendering their stability in the organic solvents.

CH– $\pi$  interactions are generally much weaker compared to hydrogen bonding and  $\pi$ – $\pi$  interactions [13]. The remarkable performance of HBPE in functionalizing and solubilizing MWCNTs and graphene is attributed its unique globular-shaped highly-

compact hyperbranched topology. The presence of abundant branch ends on its spherical surface is believed to render high-density stronger CH– $\pi$  interactions between HBPE and the nanotube surface and thus high nanotube solubility [38,48]. Following the general polymer structure–property relationships, the chain topology and molecular weight of the polymer are reasoned to be important macromolecular structural parameters governing the performance of the polymer in nanotube solubilization in this particular system. To further understand the mechanism and to elucidate the intriguing roles of chain topology and molecular weight in this unique system, we have tailor designed in this work a broad range of well-defined highly branched polyethylenes (PEs) of varying in topology and molecular weight, and have investigated systematically their effects on the solubility of MWCNTs. Meanwhile, we have also synthesized narrow-distributed PEs bearing a terminal pyrene group and investigated the possible synergistic effect arising from these additional specific groups on the nanotube solubilization.

## 2. Experimental section

### 2.1. Materials and reagents

MWCNTs (a product of Arkema Inc.) were purchased from Aldrich and used without further purification. These nanotubes were reported to have a purity of >90%, external diameter of 10–15 nm, inner diameter of 2–6 nm, length of 0.1–10  $\mu\text{m}$ , and thickness of 5–15 graphene layers. Pd–diimine catalysts, [(ArN=C(Me)–(Me)C=NAr)Pd(Me)(N=CMe)]<sup>+</sup>SbF<sub>6</sub><sup>–</sup> (**1**) and [(ArN=C(Me)–(Me)C=NAr)Pd(CH<sub>2</sub>)<sub>3</sub>CO(O)Me]<sup>+</sup>SbF<sub>6</sub><sup>–</sup> (**2**) (Ar = 2,6-(*i*Pr)<sub>2</sub>C<sub>6</sub>H<sub>3</sub>), were synthesized by following literature procedures [49]. Polymer-grade ethylene was obtained from Praxair and purified by passing through 3 Å/5 Å molecular sieves and Oxiclear columns in sequence to remove moisture and oxygen, respectively, before use. Dichloromethane (>99.9%) and chlorobenzene (>99.5%) were obtained from Fisher Scientific and purified through a solvent treatment system (Innovative Technology Inc.) before use. THF (ACS reagent, >99.0%), toluene (>99.5%), and methanol (>99.8%) were all obtained from Fisher Scientific. Chloroform (>99.8%) and *n*-heptane (>99.0%) were obtained from Aldrich. All these solvents were used as received.

### 2.2. Synthesis of pyrene-functionalized Pd–diimine catalyst (**3**)

The pyrene-functionalized Pd–diimine catalyst, [(ArN=C(Me)–(Me)C=NAr)Pd(CH<sub>2</sub>)<sub>3</sub>CO(O)(CH<sub>2</sub>)Py]<sup>+</sup>SbF<sub>6</sub><sup>–</sup> (**3**) (Ar = 2,6-(*i*Pr)<sub>2</sub>C<sub>6</sub>H<sub>3</sub>, Py = pyrenyl), was synthesized by reacting **1** with pyrenemethyl acrylate (CH<sub>2</sub>=CHCOOCH<sub>2</sub>Py) that was synthesized by following a similar literature procedure [26]. Catalyst **1** (0.95 g, 1.18 mmol) and pyrenemethyl acrylate (0.50 g, 1.75 mmol, 1.48 equiv.) were subsequently added into a 100 mL Schlenk flask containing 40 mL of anhydrous dichloromethane under nitrogen protection. The solution was stirred at room temperature for 96 h under nitrogen atmosphere. After the reaction, the resulting solution was filtered using a 0.22  $\mu\text{m}$  PTFE syringe filter. The filtrate was concentrated *in vacuo* to a volume of ca. 5 mL, and anhydrous diethyl ether (10 mL) was added to precipitate the product. The precipitate was washed with anhydrous diethyl ether for 2 times (20 mL/time), followed with drying *in vacuo* at room temperature for 2 h to render **3** as a light yellow powder (0.70 g, 56.5% yield). Anal. Calcd (found) for C<sub>49</sub>H<sub>57</sub>O<sub>2</sub>N<sub>2</sub>PdSbF<sub>6</sub>: C, 56.41(56.15); N, 2.67(2.67); H, 5.78(5.48). <sup>1</sup>H NMR (500 MHz, CD<sub>2</sub>Cl<sub>2</sub>, ppm)  $\delta$ : 7.85–8.31 (m, 9H, pyrenyl protons), 7.36–7.43 (m, 6H, H<sub>aryl</sub>), 5.03 (s, 2H, pyrenyl-CH<sub>2</sub>O), 3.10 (septet, 2H, CHMe<sub>2</sub>), 3.05 (septet, 2H, C'HM<sub>2</sub>), 2.52 (t, 2H, PdCH<sub>2</sub>CH<sub>2</sub>CH<sub>2</sub>C(O)), 2.32 and 2.30 (s, 3 each,

$N=C(Me)-(Me)C' \equiv N$ ), 1.52, 1.51, 1.44, 1.43, 1.35, 1.34, 1.29 and 1.27 (s, 3 each,  $CHMeMe'$ ,  $C'HMeMe'$ ), 1.40 (t, 2H,  $PdCH_2CH_2CH_2C(O)$ ), 0.74 (pentet, 2H,  $PdCH_2CH_2CH_2C(O)$ ).  $^{13}C$  NMR (125 MHz,  $CD_2Cl_2$ , ppm)  $\delta$ : 182.5 ( $PdCH_2CH_2CH_2C(O)$ ), 179.0 and 172.0 ( $N=C-C' \equiv N$ ), 140.5 and 140.6 (Ar, Ar',  $C_{ipso}$ ), 138.4 and 138.0 (Ar, Ar',  $C_o$ ), 129.5 and 128.6 (Ar, Ar',  $C_p$ ), 124.5 and 124.2 (Ar, Ar',  $C_m$ ), 132.4, 131.2, 130.5, 128.8, 128.5, 128.0, 127.6, 127.2, 126.5, 126.1, 125.9, 122.1, 125.3, 124.7, 124.6, 124.3 (pyrenyl carbon), 68.5 (pyrenyl- $CH_2-O$ ), 35.9 and 29.9 ( $PdCH_2CH_2CH_2C(O)$ ), 29.2 and 28.8 (CHMe,  $C'HMe$ ), 23.9 ( $PdCH_2CH_2CH_2C(O)$ ), 23.6, 23.5, 23.0 and 22.9 (CHMeMe',  $C'HMeMe'$ ), 21.4 and 19.6 ( $N=C(Me)-(Me)C' \equiv N$ ).

### 2.3. Synthesis of PEs of different topology, molecular weight, and end group

Table 1 summarizes the four sets of PEs synthesized and used in this work, along with their polymerization conditions and characterization results. In Set 1, three polymers having similar molecular weight but different chain topologies, LPE, MBPE and HBPE were synthesized with catalyst **1** under different combinations of ethylene pressure and temperature in our earlier work. Please refer to our earlier paper for their detailed polymerization procedures [50]. The polymers in Set 2 (MBPE27K ~ MBPE84K with the number indicating number-average molecular weight ( $M_n$ ) of the polymer) are narrowly distributed PEs of moderately hyperbranched chain topology with varying molecular weights, which were synthesized in our earlier work via “living” ethylene polymerization with catalyst **1** at 1 atm and 25 °C [51]. Set 3 (M-LPE8K ~ M-LPE98K) is comprised of narrowly distributed PEs of linear topology but different molecular weights with a methyl ester end group at the starting end. They were synthesized by “living” ethylene polymerization with catalyst **2** at 27 atm and 5 °C with varying polymerization time. Set 4 (P-LPE9K ~ P-LPE89K) is comprised of pyrene-ended narrow-distributed PEs of linear topology but

different molecular weights, which were synthesized with catalyst **3** at 27 atm and 5 °C with varying polymerization time. The polymerization and polymer purification procedures for the polymers in Sets 3 and 4 were similar to those we used for synthesizing the polymers in Set 2, which were reported in our earlier paper [51].

### 2.4. Noncovalent solubilization of MWCNTs with PEs in organic solvents

Noncovalent solubilization of MWCNTs was carried out in organic solvents (THF, chloroform, heptane and toluene) with various PEs via a common ultrasonication process. Typically, a mixture of MWCNTs, polymer, and solvent at a prescribed composition was added into a 25 mL glass vial and sonicated in a bath sonicator (Branson 3510 with a measured ultrasonication power of 70 W) at room temperature for 30 min. The resulting mixture was left undisturbed overnight and the supernatant was then filtered through a short plug of glass wool to give a homogeneous solution of MWCNTs. UV–Vis absorbance spectrum was subsequently taken on the dispersion after proper dilution by scanning from 190 to 900 nm (step size: 2 nm) within a 1 cm cell. The nanotube solubility was calculated from the UV–Vis absorbance at 500 nm via the Beer–Lambert law ( $A = \epsilon bc$ ) [38]. The UV–Vis extinction coefficients of 0.0488 mL/(g cm) in chloroform and 0.0477 mL/(g cm) in both THF and heptane, determined in our earlier work [38], were used for the calculation. The final nanotube solubility is the average value obtained on five individually prepared nanotube solutions.

### 2.5. Characterizations and measurements

Nuclear magnetic resonance ( $^1H$  NMR) spectra of **3** and various polymers were obtained with a Varian Gemini 2000 spectrometer or a Bruker AV500 spectrometer in  $CDCl_3$  as solvent at ambient

**Table 1**  
Synthesis of four sets of PEs varying in chain topology, molecular weight, and terminal group.

Set	PE sample	Polymerization condition			Triple-detection GPC characterization <sup>a</sup>				$^1H$ NMR analysis	
		Catalyst	Ethylene pressure and temperature	Time (h)	$M_n$ (kg/mol)	$M_w$ sc2(kg/mol)	PDI	$[\eta]_w$ (mL/g)	$M_{n,NMR}^b$ (kg/mol)	Branches <sup>c</sup> (per 1000C)
1	LPE	<b>1</b>	30 atm, 25 °C	5	114	186	1.63	71	–	102
	MBPE	<b>1</b>	6 atm, 35 °C	6	96	152	1.59	37	–	97
	HBPE	<b>1</b>	1 atm, 35 °C	18	94	156	1.66	16	–	112
2	MBPE27K	<b>1</b>	1 atm, 25 °C	1	27	28	1.03	14	–	95
	MBPE47K	2		47	51	1.09	19	–	106	
	MBPE63K	3.2		63	74	1.17	24	–	95	
	MBPE71K	4		71	87	1.24	26	–	97	
	MBPE78K	5		78	101	1.29	29	–	96	
	MBPE84K	6		84	112	1.33	31	–	94	
	M-LPE8K	<b>2</b>		27 atm, 5 °C	1	8	9	1.09	15	7
M-LPE15K	2	15	16		1.01	22	15	92		
M-LPE23K	3	22	23		1.01	28	20	95		
M-LPE29K	4	29	29		1.02	32	28	90		
M-LPE35K	5	35	36		1.03	36	38	88		
M-LPE74K	12	74	82		1.12	58	97	88		
M-LPE98K	18	98	112		1.14	69	168	86		
4	P-LPE9K	<b>3</b>	27 atm, 5 °C	1	9	9	1.00	15	7	94
	P-LPE17K	2		17	19	1.01	22	18	86	
	P-LPE23K	3		23	23	1.01	28	23	87	
	P-LPE30K	4		30	30	1.02	32	30	82	
	P-LPE36K	5		36	37	1.02	36	39	93	
	P-LPE42K	6		42	43	1.03	39	52	87	
	P-LPE77K	12		77	82	1.07	57	86	91	
	P-LPE89K	16		89	99	1.11	64	132	84	

<sup>a</sup> Number-average molecular weight ( $M_n$ ), weight-average molecular weight ( $M_w$ ), and polydispersity index (PDI) were determined with the light scattering detector within the triple-detection GPC. Weight-average intrinsic viscosity ( $[\eta]_w$ ) were measured with the viscosity detector within the triple-detection GPC.

<sup>b</sup> Number-average molecular weight ( $M_{n,NMR}$ ) determined with  $^1H$  NMR spectroscopy based on terminal group analysis.

<sup>c</sup> Total branch density determined with  $^1H$  NMR spectroscopy.

temperature. Triple-detection gel permeation chromatography (GPC) analysis of polymers was performed on a Polymer Laboratories PL-GPC 220 system equipped with a differential refractive index (DRI) detector (from Polymer Laboratories), a three-angle laser light scattering (LS) detector (high-temperature miniDAWN from Wyatt Technology) and a four-bridge capillary viscosity detector (from Polymer Laboratories). The laser detector had a wavelength of 687 nm with three scattering angles of 45, 90 and 135°. The GPC separation system was composed of one guard column (PL# 1110–1120) and three 30 cm columns (PL gel 10  $\mu$ m MIXED-B 300  $\times$  7.5 mm). HPLC-grade THF was used as the mobile phase with a flow rate of 1.0 mL/min and the whole GPC system was maintained at 33 °C. Two narrowly distributed polystyrene (PS) standards (from Pressure Chemicals, with weight-average molecular weight ( $M_w$ ) of 30,000 and 200,000 g/mol, respectively) were used for the normalization of light scattering signals and the determination of inter-detector delay volume and band broadening. Astra software from Wyatt Technology was used for collection and process of the data. A  $dn/dc$  value of 0.078 mL/g was adopted for all the PE samples.

UV–Vis absorbance spectra were recorded with an Ultra spec 2100 pro spectrophotometer. Transmission electron microscopy (TEM) measurements were performed on a Philips EM400 microscope operated at 100 keV. TEM samples were made by depositing a few drops of dilute nanotube solutions onto copper grids coated with a carbon film, followed with drying *in vacuo* for 5 min. Thermogravimetric analysis (TGA) was performed on a TA Instruments Q50 thermogravimetric analyzer under  $N_2$  atmosphere with a heating rate of 10 °C/min.

### 3. Results and discussion

#### 3.1. Effect of polymer chain topology

To examine the effect of polymer chain topology on the nanotube solubilization, we used a set of three branched PE homopolymers varying in chain topology (Set 1 in Table 1), including LPE, MBPE, and HBPE, for the noncovalent nonspecific solubilization of MWCNTs. These three samples were synthesized via chain walking ethylene polymerization with Pd–diimine catalyst **1** under different combinations of ethylene pressure and temperature (30 atm/25 °C, 6 atm/35 °C, and 1 atm/35 °C, respectively) [50]. Following the well-established chain walking mechanism of Pd–diimine catalysts [44,45], the topology of resulting PEs in this unique polymerization system depends sensitively on ethylene pressure and temperature, with an increasingly hyperbranched topology yielded with decreasing ethylene pressure and/or increasing temperature. The three polymers should have increasingly compact chain topology in the order from LPE to MBPE and to HBPE, with LPE being typically linear in topology but containing mainly short branches, MBPE being moderately hyperbranched, and HBPE being hyperbranched, as well elucidated in our earlier papers [50]. Their Mark–Houwink curves (intrinsic viscosity vs. molecular weight) in Fig. 1 confirms the topological differences among the three samples, with the intrinsic viscosity curve consistently shifted down following the above order. Scheme 1(a) depicts schematically the topological differences among the three PEs. Despite their very different chain topologies, this set of polymers have very similar average molecular weights and molecular weight distribution with  $M_n$  being about 100 kg/mol and polydispersity index (PDI) being about 1.6. Meanwhile, they also have similar total branch density of about 100 branch ends per 1000 carbons as per characterization with  $^1H$  NMR spectroscopy (see Table 1). These features make them well suited for the elucidation of the effect of chain topology on nanotube solubility.

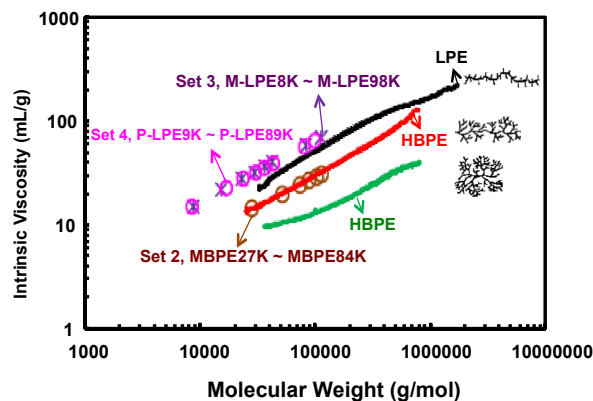
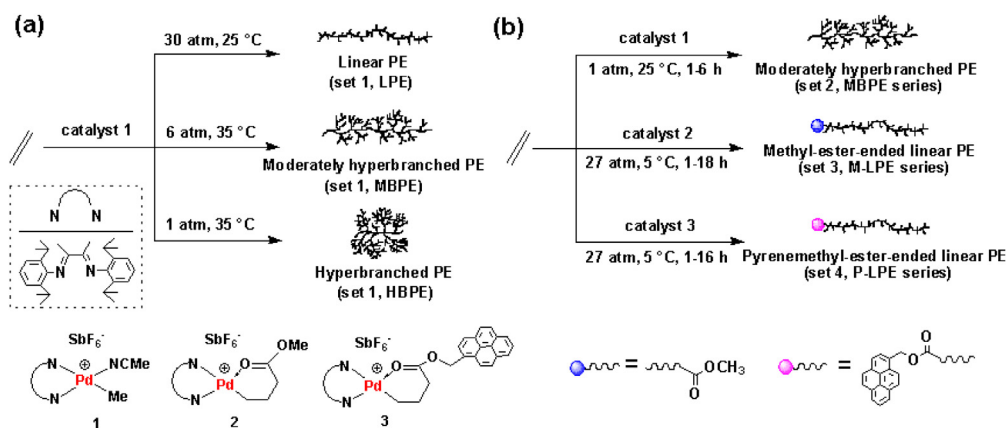


Fig. 1. Mark–Houwink plots of the four sets of PE samples, constructed with the intrinsic viscosity and molecular weight data measured with triple-detection GPC using THF as the eluant at 33 °C.

Noncovalent solubilization of MWCNTs with the three PE samples was performed in four common low-polarity organic solvents (chloroform, THF, *n*-heptane, toluene), in which all the polymers show good and increasing solubility following the order at room temperature. With each polymer in any given solvent, four different polymer/MWCNT mass ratios ( $m_{PE}/m_{NT} = 1, 2.5, 5, 7.5$ , respectively) were adopted at a fixed MWCNT feed concentration (2 mg in 1 mL solvent). A common procedure, including sonication, settlement, and filtration under identical conditions, was used to obtain nanotube solutions. Negligible nanotube solubility was achieved when toluene or *n*-heptane was used as the solvent with all three polymers. On the contrary, dark nanotube solutions were obtained with the polymers in THF or chloroform. Some of solutions, particularly those prepared at high  $m_{PE}/m_{NT}$  ratios were found stable without nanotube settling even after two years. This distinct solvent effect has been found in our earlier studies [38,48] and should be attributed to high polymer–solvent interactions in toluene or *n*-heptane since the polymers dissolve better in them, which renders insufficient polymer adsorption on nanotubes and thus ineffective nanotube solubilization.

The nanotube concentration ( $C_{NT}$ ) in the solutions obtained with the three polymers in THF or chloroform was quantified from their UV–Vis absorbance at 500 nm after proper dilution by following the Beer–Lambert law. The extinction coefficients of 0.0477 L/(mg cm) in THF and 0.0488 L/(mg cm) in chloroform, which were determined in our earlier work for the same MWCNTs used herein [38], were used in the calculations. Fig. 2 compares  $C_{NT}$  data (average data of five solutions prepared individually at each  $m_{PE}/m_{NT}$  ratio) achieved with the three polymers differing in chain topology. In both solvents,  $C_{NT}$  increases significantly with the change of polymer topology from linear to hyperbranched, i.e., from LPE to MBPE and to HBPE, at nearly every  $m_{PE}/m_{NT}$  ratio. For example, in THF at the  $m_{PE}/m_{NT}$  ratio of 5,  $C_{NT}$  increases from 106 mg/L with LPE to 255 mg/L with MBPE and to 653 mg/L with HBPE. In chloroform at the  $m_{PE}/m_{NT}$  ratio of 5,  $C_{NT}$  increases from 47 mg/L with LPE to 563 mg/L with MBPE and to 880 mg/L with HBPE. This clear trend of change in  $C_{NT}$  confirms the significant effect of chain topology on nanotube solubilization with the use of this class of highly branched PEs. Consistent with our earlier findings [38], the  $C_{NT}$  data are generally higher in chloroform than the corresponding ones achieved in THF with each polymer at an identical  $m_{PE}/m_{NT}$  ratio. Along with the negligible nanotube solubilization in toluene and *n*-heptane noted above, this also indicates the dramatic effect of the solvent on nanotube solubilization with this set of polymers by changing the polymer–solvent interactions. With a given polymer in either solvent, increasing the  $m_{PE}/m_{NT}$  ratio from 1 to 5 generally



**Scheme 1.** Synthesis of the four sets of PEs, (a) Set 1 and (b) Sets 2–4, differing in chain topology, molecular weight, and end group by ethylene polymerization catalyzed with various Pd–diimine catalysts.

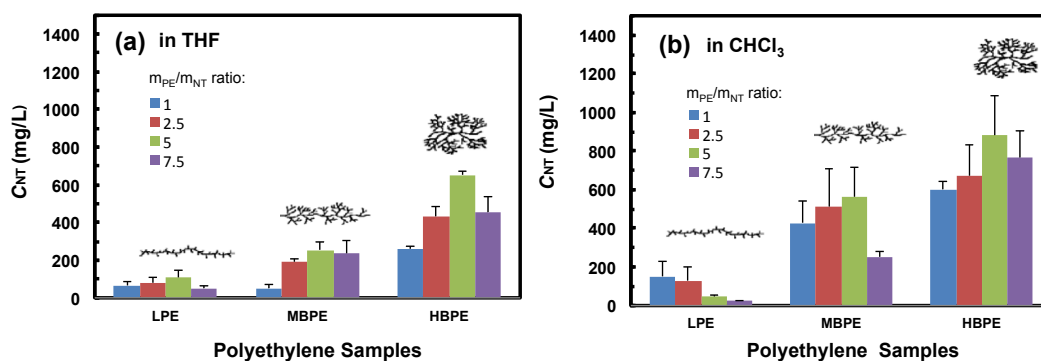


**Fig. 2.** Nanotube solubility achieved with PEs in Set 1 (i.e., LPE, MBPE, and HBPE) in THF (a) and chloroform (b), respectively, at different  $m_{PE}/m_{NT}$  ratios and but the same nanotube feed concentration of 2 mg/mL.

leads to an increase in  $C_{NT}$ , which should be attributed to the increased adsorption of the polymer on the nanotubes. A continued increase from 5 to 7.5 somehow results in a slight drop in  $C_{NT}$ , a phenomenon also observed in our earlier studies on nanotube and graphene solubilization with HBPE at enhanced loadings [38,48].

Fig. 3 shows representative TEM images of the solubilized nanotubes achieved with the use of LPE. Despite the lowest  $C_{NT}$  data achieved with LPE among the three polymers, the solubilized nanotubes are well exfoliated and debundled from each other, with

the presence of individual nanotubes and the absence of large aggregates. Similar images were also seen with the nanotubes solubilized with the use of more efficient HBPE or MBPE. In contrast to the severely aggregated pristine MWCNTs [38], these images confirm the successful exfoliation and debundling of the nanotubes with the use of the polymers.

Given the absence of any specific functionality in the polymers, the mechanism of nanotube solubilization should be ascribed to the adsorption of the polymers through CH– $\pi$  interactions between

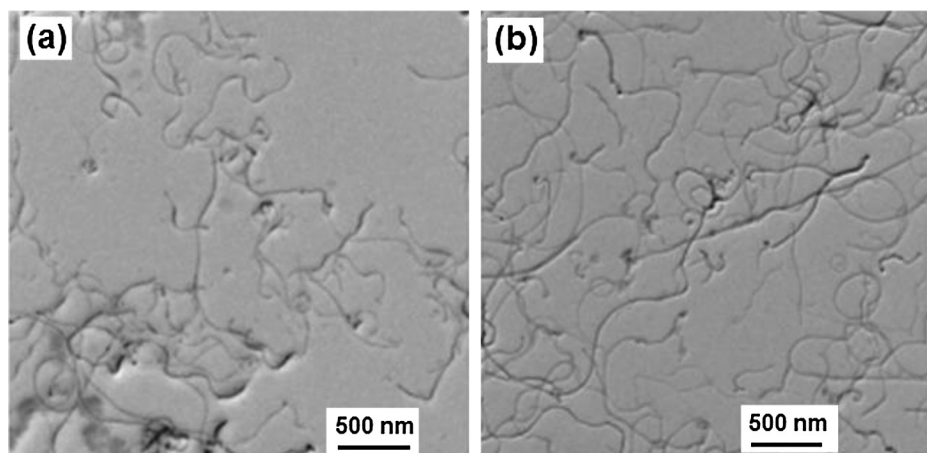


**Fig. 3.** TEM images of solubilized nanotubes obtained with LPE in THF (a) and chloroform (b) at the  $m_{PE}/m_{NT}$  ratio of 1.

the polymers and nanotube sidewalls, which renders a polymer barrier against the aggregation of the nanotubes. In the case with HBPE, its adsorption on MWCNTs has been directly observed with TEM and also confirmed with TGA in our earlier work. To also confirm the adsorption of LPE on the nanotubes herein, two nanotube solutions obtained with LPE at the  $m_{PE}/m_{NT}$  ratio of 5 were filtered and washed extensively with the fresh solvent (to remove free nonadsorbed polymer) to render two LPE/MWCNT composites. Fig. 4 shows the TGA curves of the composites, along with that for pristine MWCNTs. A weight loss of about 20% mainly in the temperature range of 400–500 °C is observed in the TGA curves for both composites, confirming the presence of adsorbed LPE on nanotubes since pristine MWCNTs have no/negligible weight loss within this temperature range. Similar weight loss was also found in the HBPE/MWCNT composites prepared under identical conditions as shown in our earlier paper [38]. It should be noted that the weight loss found in these composites should belong to polymers irreversibly adsorbed on the nanotubes. Their dramatically different  $C_{NT}$  data, while at similar amounts of irreversibly adsorbed polymer, suggest that those reversibly adsorbed polymer in the solution may play an important role in facilitating nanotube solubilization. In the nanotube solutions, such reversibly adsorbed polymers should be present. But their quantification is not possible currently.

With the above results, we now discuss the mechanism in the effect of solvent on  $C_{NT}$  in this unique system. Extensive investigations have been performed in the literature on elucidating the effects of solvent and the use of polymer on the solubilization of carbon nanotubes and graphene [3,52–59]. In the case of the solubilization of carbon nanotubes or graphene in a pure solvent without any additive (polymer, surfactant, etc.), theoretical thermodynamic derivations, confirmed with experimental evidences, indicate that a good solvent should have a solubility parameter ( $\delta_S$ ) close to that ( $\delta_{NT} = 21.25 \text{ MPa}^{1/2}$ ) of the nanotubes or graphene. In such good solvents, the enthalpy of mixing is minimized so as to render effective solubilization of the nanotubes or graphene at high concentrations [3,58,59].

In the case of polymer-assisted noncovalent solubilization of nanotubes/graphene, the solvent, like those used herein ( $\delta_S = 18.7, 18.5, 18.3,$  and  $15.3 \text{ MPa}^{1/2}$  for chloroform, THF, toluene, and *n*-heptane, respectively), is often not a good one for the nanotubes/graphene with an unmatched solubility parameter but is good for dissolving the polymer. To achieve nanotube solubilization, the polymer should partially adsorb on the surface at some sites while with the rest of chain segments/loops protruding into the solvent to provide steric stabilization [60]. For a given surface, there is a

competition for adsorption between polymer and solvent. For successful partial adsorption of the polymer to occur, the two competing interactions, i.e., the polymer–surface interactions leading to adsorption and the polymer–solvent interactions resulting in desorption, should be similar [60].

Coleman et al. have modeled polymer adsorption and derived a simple expression in terms of the Hildebrand solubility parameters to quantify the effects of the polymer stabilizer and solvent on the concentration of the exfoliated nanosheets [60]. Also applicable to the nanotubes, it is accordingly modified as below.

$$C_{NT} \propto \exp \left[ - \left( \frac{(\delta_S - \delta_P)(\delta_{NT} - \delta_S)}{kT} \right)^2 \right] \quad (1)$$

where  $k$  is Boltzmann constant;  $T$  is the temperature;  $\delta_S, \delta_{NT}, \delta_P$  are the solubility parameter for the solvent, nanotube, and polymer, respectively. With this expression, Coleman et al. have predicted that the concentration of exfoliated nanosheets/nanotubes is maximized if the three solubility parameters are very close, which was supported by experimental evidences in their study of exfoliated graphene [60]. We also attempted to use Eq. (1) to semi-quantitatively examine the effect of solvent on the  $C_{NT}$  value herein. Given that they are constructed solely with ethylene sequences, we take the solubility parameter of regular PE,  $16.1 \text{ MPa}^{1/2}$ , for the three branched PEs herein [48]. Following Eq. (1), the  $C_{NT}$  value achieved with the use of either polymer in the four different solvents herein should increase in the order: chloroform < THF < toluene < *n*-heptane. This differs from the experimental results herein. Possibly, Eq. (1) is oversimplified and does not fit this particular system herein.

The completely inefficient nanotube solubilization in toluene and *n*-heptane with all three polymers indicates the absence of sufficient polymer adsorption for steric stabilization. This should result from the excessively strong polymer–solvent interactions in these two solvents since these two solvents have closer solubility parameters to that of PEs and are better solvents for PEs [25,32,38]. From the higher  $C_{NT}$  values achieved in chloroform than in THF with each polymer in this set, we reason that the polymer–solvent interactions in chloroform are more appropriately suited for polymer adsorption than in THF.

We further discuss the mechanism in the effect of polymer chain topology on  $C_{NT}$  in this system. Given their identical chemical composition, the three PEs in this set, though having different chain topologies, should have a similar/identical solubility parameter. With this, Eq. (1) obtained through simplified modeling is futile in explaining the effect of polymer chain topology on  $C_{NT}$  in a given solvent. We reason that chain topology affects the polymer–solvent interactions and subsequently the polymer adsorption and  $C_{NT}$ , with more linearized chain topology rendering stronger polymer–solvent interactions and thus reduced polymer adsorption. As proposed in our earlier work [38], the globular-shaped HBPE (having a hydrodynamic diameter at about 10 nm) should adsorb onto the nanotube sidewall surface at some of its spherical sites with the rest of the globule protruding into the solvent (see Scheme 2). Due to the highly compact chain conformation and congested spherical surface of HBPE, the polymer–solvent interactions are expected to be weaker; meanwhile, the interactions between the adsorbed and nonadsorbed HBPE globules via physical chain entanglements should also be negligible. In the case with the adsorbed LPE, the linear protruding chain segments/loops are expected to have stronger interactions with the solvent due to less compact chain conformation and there is enhanced possibility of chain entanglements between the nonadsorbed and adsorbed chains (Scheme 2). On the other hand, increasing the chain compactness

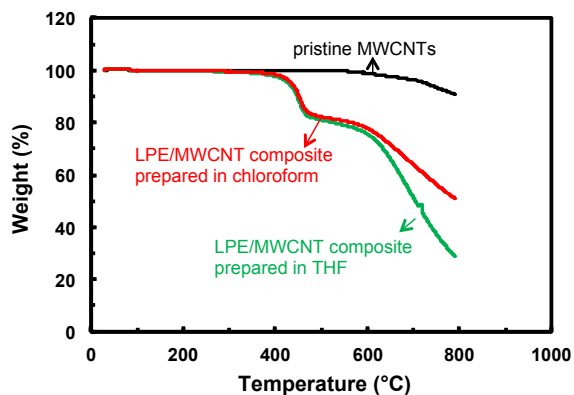
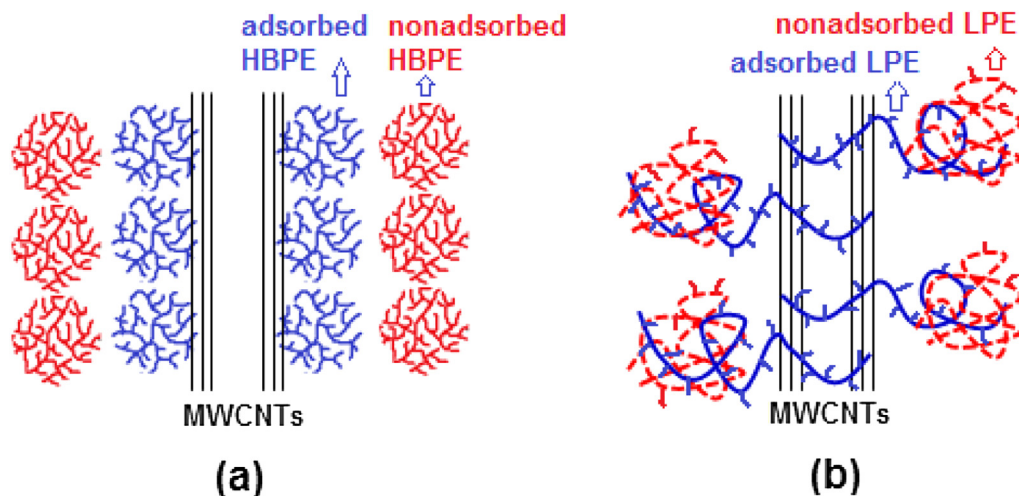


Fig. 4. TGA curves for pristine MWCNTs, and the LPE/MWCNT composites prepared in chloroform and THF, respectively. The free polymer was removed from both two composites.



**Scheme 2.** Proposed noncovalent interactions between MWCNTs and globular HBPE (a) and linear LPE (b) in organic solvents.

from LPE to HBPE is also reasoned to lead to enhanced polymer–nanotube interactions since the density of chain segments per volume is enhanced.

Carbon nanotubes have been extensively demonstrated to induce crystallization of crystalline polymers, such as high-density polyethylene (HDPE), in the solution to form nanohybrid shish kebabs morphology [61–63]. Due to their highly branched structures, the Pd–diimine PEs used herein are noncrystalline under the current conditions. As we have shown earlier [44], similar Pd–diimine PEs typically crystallize at around  $-30\text{ }^{\circ}\text{C}$  in the melt state. The nanotube-induced polymer crystallization should be absent in the current system with the polymers used herein, which is otherwise expected to affect the nanotube solubility.

### 3.2. Effect of polymer molecular weight

In order to investigate the effect of polymer molecular weight on  $C_{\text{NT}}$ , two sets (Sets 2 and 3 in Table 1) of narrow-distributed PEs of well-defined molecular weights were synthesized and used for the noncovalent nanotube exfoliation. Their synthesis benefits from the unique “living” feature of Pd–diimine-catalyzed ethylene polymerization at a low temperature ( $25\text{ }^{\circ}\text{C}$  or lower), where the control of molecular weight was achieved simply by tuning the polymerization time [45]. The polymers in Set 2, MBPE27K ~ MBPE84K (with the number indicating  $M_n$ ) synthesized with **1** at 1 atm/ $25\text{ }^{\circ}\text{C}$  [51], have nearly identical moderately hyperbranched chain topology as MBPE in Set 1 since their intrinsic viscosity data locate on the curve for MBPE (see Fig. 1). The narrow-distributed polymers in Set 3, M-LPE8K ~ M-LPE98K (with M standing for methyl-ester-ended PEs and the number indicating  $M_n$ ) were synthesized with catalyst **2** at 27 atm/ $5\text{ }^{\circ}\text{C}$ . Following the characteristic chain initiation chemistry of chelate catalyst **2** (see Scheme 1(b)) [45], each polymer in Set 3 should contain about a methyl ester functionality at the starting end (representatively, see Fig. 5 for the  $^1\text{H}$  NMR spectrum of M-LPE23K), which is confirmed by end group analysis. Meanwhile, the polymers in Set 3 have the similar linear topology of LPE in Set 1 as per their intrinsic viscosity data (see Fig. 1). From GPC characterization, these two sets of polymers all have narrow molecular weight distribution with PDI generally below or around 1.2. All the polymers have a similar branching density of about 90 branch ends per 1000 carbons. Due to the deteriorated “living” behavior of Pd–diimine catalysts at the elevated temperature of  $35\text{ }^{\circ}\text{C}$  [51], synthesis of narrow-distributed

PEs of controllable molecular weight with chain topology resembling HBPE was not possible.

Noncovalent solubilization of MWCNTs was performed with these two sets of narrow-distributed PEs at the  $m_{\text{PE}}/m_{\text{NT}}$  ratio of 5 by following the same procedure used above. Consistent with above results, negligible nanotube solubilization was achieved in toluene or *n*-heptane with any polymer in the two sets while stable solutions were obtained in THF and chloroform. Fig. 6 plots and compares the  $C_{\text{NT}}$  data as a function of  $M_n$  obtained with the two sets of polymers in THF and chloroform, respectively. In particular, one can see a strong dependence of  $C_{\text{NT}}$  on molecular weight with polymers in Set 3. In both THF and chloroform,  $C_{\text{NT}}$  increases initially to a peak value, then followed with a consistent decrease, with the gradual increase of  $M_n$  from 8 to 98 kg/mol in Set 3. The peak-maximum  $C_{\text{NT}}$  value (689 mg/L in THF and 655 mg/L in chloroform) occurs at the  $M_n$  value of ca. 29 kg/mol in THF and 15 kg/mol in chloroform. At  $M_n > 74\text{ kg/mol}$ , the  $C_{\text{NT}}$  values are very low, i.e., ca. 50 mg/mL in THF and 17 mg/mL in chloroform, which in good agreement with the low  $C_{\text{NT}}$  values (106 mg/L in THF and 47 mg/L in chloroform) found with the broad-distributed LPE of similar  $M_n$  in the above section. These results indicate that PEs of

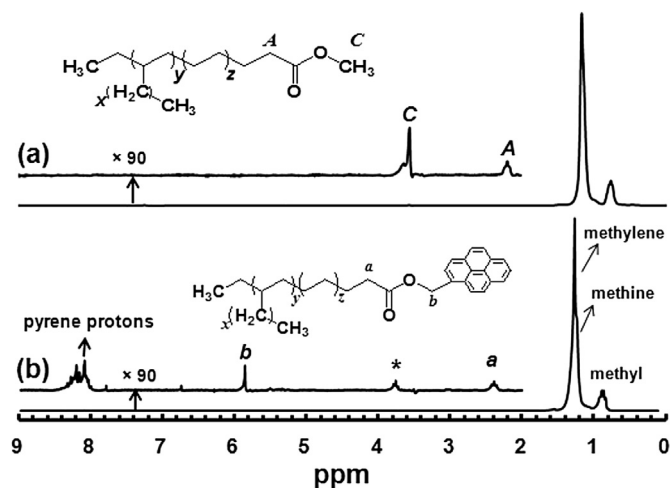


**Fig. 5.**  $^1\text{H}$  NMR spectra of methyl-ester-ended M-LPE23K (a) in Set 3 and pyrenemethyl-ester-ended P-LPE23K (b) in Set 4.

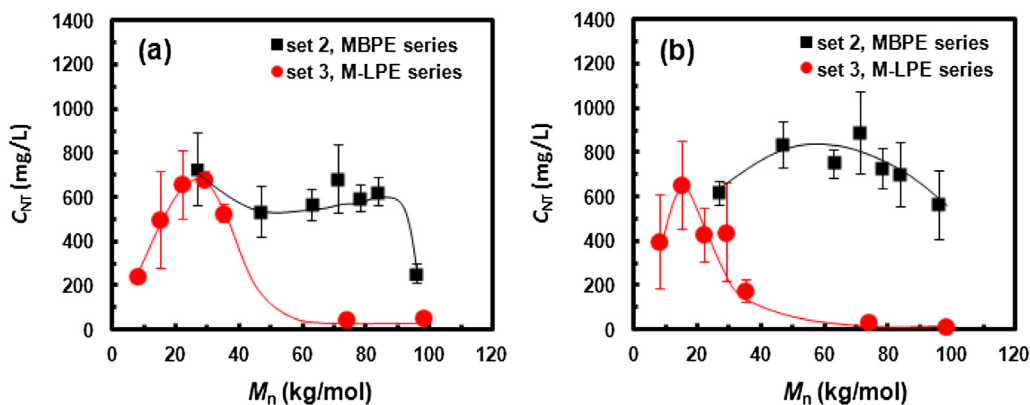


Fig. 6.  $C_{NT}$  as functions of polymer  $M_n$  for nanotube solutions obtained with the polymers in Set 2 (MBPE series) and Set 3 (M-LPE series), respectively, in THF (a) and chloroform (b) at the  $m_{PE}/m_{NT}$  ratio of 5.

linear topology also can efficiently solubilize the MWCNTs in both solvents at high concentrations, provided that they have appropriate molecular weights. The trend of change in  $C_{NT}$  with this set of polymers is hypothesized to result from the subtle change in polymer–solvent interactions with the increase of  $M_n$  in this set of linear polymers. At very low  $M_n$  values (e.g., <8 kg/mol), we reason that the chain segments (of an adsorbed chain) protruding into the solvent are relatively too short to provide sufficient barrier against nanotube aggregation. The initial increase in  $M_n$  thus leads to a thicker barrier, which better help the stabilization of the dispersed MWCNTs. On the contrary, too high  $M_n$  leads to the pulling-off or desorption of the adsorbed chain due to the excessively enhanced polymer–solvent interactions [25,32,38].

In the case with polymers in Set 2 of a more compact chain topology, the dependence of  $C_{NT}$  on  $M_n$  is much weaker without a clear conclusive pattern at the low molecular weight end with the range of polymers herein. Nevertheless, at the high molecular weight end,  $C_{NT}$  shows a trend of slight decrease with the increase of  $M_n$ , which is also indicative of polymer desorption due to excessively enhanced polymer–solvent interactions. However, at  $M_n > 40$  kg/mol,  $C_{NT}$  data achieved with polymers in Set 2 (MBPE series) are much higher than those achieved with the counter polymers in Set 3 (M-LPE series) due to more compact chain topology, which is also in good agreement with the results obtained in the above section. These indicate that the polymer–solvent interactions show a weaker dependence on  $M_n$  with Set 2 polymers of more compact chain topology.

### 3.3. Effect of terminal pyrene group

We further investigate the effect of the presence an additional pyrene end group in the branched PEs on the nanotube solubility. Pyrene and similar functionalities have been well demonstrated to show noncovalent specific  $\pi$ – $\pi$  interactions with nanotube sidewalls and polymers containing these functionalities have been extensively applied to render nanotube solubilization in organic solvents [1–10,13,14,25–32]. Herein, we designed a set of narrow-distributed PEs (Set 4 in Table 1, P-LPE9K ~ P-LPE89K with P standing for pyrene-ended chains and the number indicating  $M_n$ ) containing a pyrenemethyl ester group at the starting end by “living” ethylene polymerization with catalyst **3** at 27 atm/5 °C (see Scheme 1b). Catalyst **3**, having the pyrene group designed specifically into its initiating end, was synthesized by reacting **1** with pyrenemethyl acrylate ( $CH_2=CHCOOCH_2Py$ ) following the same reaction chemistry used for synthesis of **2** and other various functionalized Pd–diimine ester chelate catalysts our group

synthesized earlier [45]. End-group analysis with  $^1H$  NMR spectroscopy of the polymers (see Fig. 5 for a representative  $^1H$  NMR spectrum) confirms that nearly each chain contains a pyrene end, with their  $M_n$  values determined through NMR end-group analysis generally in good agreement with those determined with light scattering in triple-detection GPC analysis (see Table 1). Meanwhile, this set of polymers is also featured with low PDI (around or below 1.1). From Fig. 1, the intrinsic viscosity data of this set of polymers locate on the same line as those for polymers in Set 3, indicative of the identical linear topology of these two sets of polymers given the same polymerization conditions. Like those in Set 3, polymers in Set 4 also have similar branching density with ca. 90 branch ends per 1000 carbons.

Noncovalent solubilization of MWCNTs was carried out with polymers in Set 4 at the  $m_{PE}/m_{NT}$  ratio of 5 in all four solvents (THF, chloroform, *n*-heptane, and toluene). Different from previous sets of polymers, we expect the possible involvement of both nonspecific CH– $\pi$  and specific  $\pi$ – $\pi$  interactions between the polymers in Set 4 and the nanotubes when used for noncovalent solubilization of the MWCNTs, with the former resulting from the polymer backbone and the latter from the pyrene end group. The involvement of the specific  $\pi$ – $\pi$  interactions may possibly provide additional synergistic effects on  $C_{NT}$ . This is confirmed to be the case when nanotube solubilization was carried out with the polymers in *n*-heptane. Dark nanotube solutions with significant  $C_{NT}$  values (ca. 100–400 mg/L calculated by using the extinction coefficient of 0.0477 L/(mg cm) in THF) were successfully obtained while it was not possible with all the other sets of polymers without having the specific functionality. Fig. 7a shows the dependence of  $C_{NT}$  on  $M_n$  with the set of polymers in *n*-heptane. One can see an initial increase of  $C_{NT}$ , followed with a decrease, with the increase of  $M_n$ , which reflect again the gradual increase of polymer–solvent interactions. The highest  $C_{NT}$  value of 407 mg/L was achieved with P-LPE23K at  $M_n$  of 23 kg/mol. These  $C_{NT}$  data clearly confirms the presence of specific  $\pi$ – $\pi$  interactions with these polymers having a pyrene end group in *n*-heptane. Meanwhile, the  $\pi$ – $\pi$  interactions are reasoned to be the sole ones leading to nanotube solubilization since CH– $\pi$  interactions, as demonstrated above, are ineffective to render nanotube solubility in the solvent. Fig. 7b shows a TEM image of the solubilized nanotubes obtained with P-LPE23K. Debundled individual nanotubes are clearly seen, confirming the successful nanotube exfoliation and solubilization. Meanwhile, it is also noted from Fig. 7a that significant  $C_{NT}$  values at ca. 200 mg/L are still maintained even with polymers of high  $M_n$ 's (77 and 89 kg/mol). This is distinctly different from the negligible  $C_{NT}$  values achieved in THF or chloroform with M-LPE series (Set 3) of

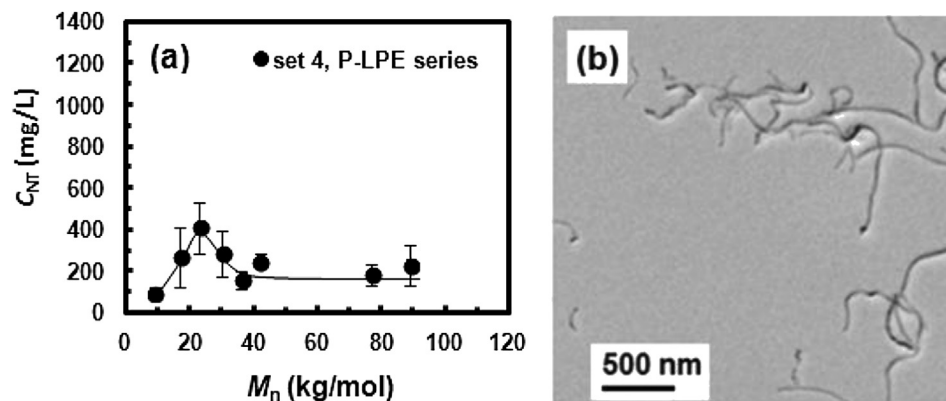


Fig. 7. (a)  $C_{NT}$  as a function of  $M_n$  for nanotube solutions obtained with the polymers in Set 4 (P-LPE series) in *n*-heptane at the  $m_{PE}/m_{NT}$  ratio of 5; (b) TEM image of solubilized nanotubes obtained with the P-LPE23K in Set 4 in *n*-heptane at the  $m_{PE}/m_{NT}$  ratio of 1.

polymers at similar molecular weights. It confirms that specific  $\pi$ – $\pi$  interactions between the pyrene end group and nanotube sidewalls are much stronger than the nonspecific CH– $\pi$  interactions. Despite the success in *n*-heptane, negligible nanotube solubilization was achieved with any polymers in Set 4 in toluene. This once again should result from insufficient polymer adsorption due to the over-strong polymer–solvent interactions in toluene since it is the best solvent among the four for the polymers.

We further investigate the nanotube solubilization with polymers in Set 4 in THF and chloroform. Fig. 8 shows  $C_{NT}$  data obtained with polymers in Set 4 in THF and chloroform, respectively. Those achieved above with polymers in Set 3 (i.e., M-LPE series) under identical conditions are also included in Fig. 8 for comparison to investigate the effect of end group, since these two sets of polymers have identical linear chain topology and similar molecular weight range but different end group. In general, there are no distinct differences in the  $C_{NT}$  data in both solvents with the polymers from the two different sets at similar molecular weight. However, a weak but notable trend with polymers in Set 4 is that high  $C_{NT}$  values (ca. 676 mg/L) were obtained in THF even with polymers of low molecular weight (9 kg/mol). With the increase of  $M_n$  from 9 to 42 mg/L,  $C_{NT}$  does not show distinct changes in both solvents. But low  $C_{NT}$  data (ca. 42 mg/L in chloroform and ca. 30 mg/L in THF) were obtained with P-LPE77K and P-LPE89K of higher molecular weights in the set, which is similar with M-LPE set of polymers at similar  $M_n$  values and is indicative of insufficient polymer adsorption due to stronger polymer–solvent interactions at higher polymer molecular weights. From the marginal differences in  $C_{NT}$  data with the

two sets of polymers, we reason that CH– $\pi$  interactions should still be the predominant ones effecting the nanotube solubilization in these two solvents with polymers in Set 4. With the absence of distinguishable  $\pi$ – $\pi$  interactions in THF and chloroform, this is different from the case seen above in *n*-heptane. We suspect that, in chloroform and THF, the polymer coils are not fully relaxed and the pyrene end groups may be buried within the coils without getting exposed to the nanotube sidewalls, thus rendering insufficient  $\pi$ – $\pi$  interactions. On the contrary, the polymer coils are more relaxed in *n*-heptane with the pyrene group exposable to the nanotube surface for interactions given that *n*-heptane is a better solvent for the polymers than THF and chloroform.

#### 4. Conclusions

Four sets of highly branched Pd–diimine polyethylenes varying in structural parameters (including chain topology, molecular weight, and end group) were designed/synthesized in this work for the noncovalent solubilization of MWCNTs in four different solvents (THF, chloroform, *n*-heptane, and toluene). The three structural parameters as well as the solvent have been demonstrated to exert complex sensitive effects on the nanotube solubility. With the polymers in Set 1 of different chain topology but similar high molecular weight ( $M_n = 100$  kg/mol), we have found that changing the chain topology from linear (LPE) to moderately hyperbranched (MBPE) and to hyperbranched (HBPE) leads to significantly enhanced  $C_{NT}$  values in both THF and chloroform. With narrow-distributed polymers of linear topology in Set 3 (M-LPE series), it is

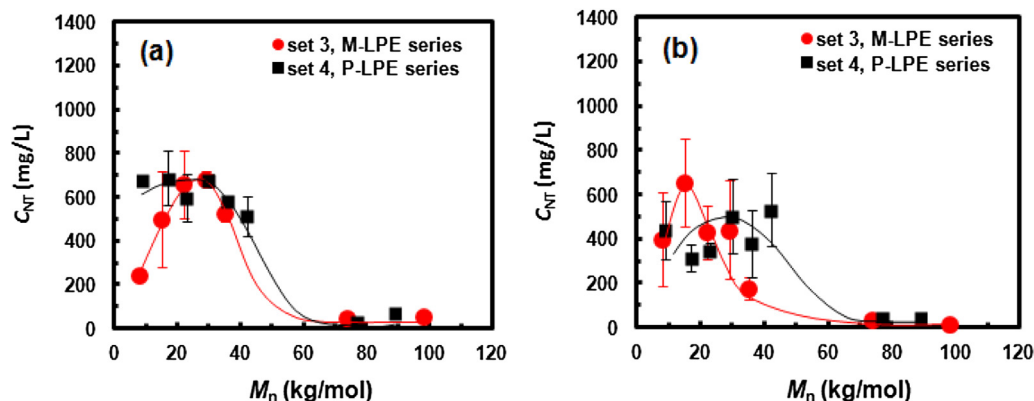


Fig. 8.  $C_{NT}$  as functions of polymer  $M_n$  for nanotube solutions obtained with the polymers in Set 3 (M-LPE series) and Set 4 (P-LPE series), respectively, in THF (a) and chloroform (b), at a fixed  $m_{PE}/m_{NT}$  ratio of 5.

demonstrated that their  $M_n$  (8–98 kg/mol) shows a dramatic effect on  $C_{NT}$  in both THF and chloroform, with high  $C_{NT}$  values (689 and 655 mg/L in THF and chloroform, respectively) achievable at optimum  $M_n$  (29 and 15 kg/mol in THF and chloroform, respectively). Too low or too high  $M_n$  leads to low  $C_{NT}$  values due to insufficient polymer barrier layer or excessive polymer–solvent interactions. For the case with narrow-distributed moderately hyperbranched polymers in Set 2 (MBPE series), their  $M_n$  (27–84 kg/mol) has no distinguishable effects on  $C_{NT}$  in both THF and chloroform, generally with high  $C_{NT}$  values (600–800 mg/L) maintained across the whole  $M_n$  range except a slight decrease at the high molecular weight end. All the polymers in Sets 1–3 were found ineffective for the nanotube solubilization in *n*-heptane and toluene due to insufficient polymer adsorption as a result of excessive polymer–solvent interactions in these two solvents. With the narrow-distributed pyrene-ended polymers in Set 4, nanotube solubilization was, however, made possible in *n*-heptane through the stronger specific  $\pi$ – $\pi$  interactions. Therein, the  $C_{NT}$  value shows a distinct dependence on  $M_n$ , with a high  $C_{NT}$  value (407 mg/L) obtained at the optimum  $M_n$  (23 kg/mol). Nevertheless, such  $\pi$ – $\pi$  interactions were found negligible when THF or chloroform was used as the solvent, where nanotube solubilization was achieved still through primarily nonspecific CH– $\pi$  interactions. Meanwhile, it was still not possible to disperse the nanotubes in toluene with these pyrene-ended polymers also due to excessively strong polymer–solvent interactions.

### Acknowledgment

The financial support for this work from the Natural Sciences and Engineering Research Council of Canada, the Canadian Foundation for Innovation (CFI), and the Canada Research Chair (CRC) is greatly appreciated. L.X. thanks the Ontario Ministry of Economic Development and Innovation for awarding a postdoctoral fellowship and the National Natural Science Foundation of China (#21074117) for funding support.

### References

- [1] Singh P, Campidelli S, Giordani S, Bonifazi D, Bianco A, Prato M. *Chem Soc Rev* 2009;38:2214.
- [2] Karousis N, Tagmatarchis N, Tasis D. *Chem Rev* 2010;110:5366.
- [3] Coleman JN. *Adv Funct Mater* 2009;19:3680.
- [4] Kharisov BI, Kharisova OV, Gutierrez HL, Méndez UO. *Ind Eng Chem Res* 2009;48:572.
- [5] Kim SW, Kim T, Kim YS, Choi HS, Lim HJ, Yang SJ, et al. *Carbon* 2012;50:3.
- [6] Tasis D, Tagmatarchis N, Bianco A, Prato M. *Chem Rev* 2006;106:1105.
- [7] Mittal V, editor. *Surface modification of nanotube fillers*. Weinheim: Wiley-VCH; 2011.
- [8] Adeli M, Soleyman R, Beiranvand Z, Madani F. *Chem Soc Rev* 2013;42:5231.
- [9] Sun J-T, Hong C-Y, Pan C-Y. *Polym Chem* 2011;2:998.
- [10] Szleifer I, Yerushalmi-Rozen R. *Polymer* 2005;46:7803.
- [11] Sakellariou G, Priftis D, Baskaran D. *Chem Soc Rev* 2013;42:677.
- [12] Homenick CM, Lawson G, Adronov A. *Polym Rev* 2007;47:265.
- [13] Bilalis P, Katsigiannopoulos D, Avgeropoulos A, Sakellariou G. *RSC Adv* 2014;4:2911.
- [14] Zhao Y-L, Stoddart JF. *Acc Chem Res* 2009;42:1161.
- [15] Pang X, Imin P, Zhitomirsky I, Adronov A. *Macromolecules* 2010;43:10376.
- [16] Imin P, Imit M, Adronov A. *Macromolecules* 2011;44:9138.
- [17] Lee HW, Yoon Y, Park S, Oh JH, Hong S, Liyanage LS, et al. *Nat Commun* 2011;2:541.
- [18] Nish A, Hwang J-Y, Doig J, Nicholas RJ. *Nat Nanotech* 2007;2:640.
- [19] Star A, Stoddart JF, Steuerman D, Diehl M, Boukai A, Wong EW, et al. *Angew Chem Int Ed* 2001;40:1721.
- [20] Star A, Liu Y, Grant K, Ridvan L, Stoddart JF, Steuerman DW, et al. *Macromolecules* 2003;36:553.
- [21] Chen Y, Malkovskiy A, Wang X-Q, Lebron-Colon M, Sokolov AP, Perry K, et al. *ACS Macro Lett* 2012;1:246.
- [22] Lee JU, Huh J, Kim KH, Park C, Jo WH. *Carbon* 2007;45:1051.
- [23] Zhao H, Yuan WZ, Tang L, Sun JZ, Xu H, Qin A, et al. *Macromolecules* 2008;41:8566.
- [24] Zou J, Khondaker SI, Huo Q, Zhai L. *Adv Funct Mater* 2009;19:479.
- [25] Gómez FJ, Chen RJ, Wang D, Waymouth RM, Dai H. *Chem Commun* 2003;190.
- [26] Lou X, Daussin R, Cuenot S, Duwez A-S, Pagnoulle C, Detrembleur C, et al. *Chem Mater* 2004;16:4005.
- [27] Yuan WZ, Mao Y, Zhao H, Sun JZ, Xu HP, Jin JK, et al. *Macromolecules* 2008;41:701.
- [28] Bahun GJ, Wang C, Adronov A. *J Polym Sci Part A: Polym Chem* 1941;2006:44.
- [29] Bahun GJ, Adronov A. *J Polym Sci Part A: Polym Chem* 2010;48:1016.
- [30] Meuer S, Braun L, Zentel R. *Chem Commun*; 2008:3166.
- [31] Meuer S, Braun L, Schilling T, Zentel R. *Polymer* 2009;50:154.
- [32] Yang L-P, Pan C-Y. *Macromol Chem Phys* 2008;209:783.
- [33] Rouse JH, Lillehei PT. *Nano Lett* 2003;3:59.
- [34] Mamedov AA, Kotov NA, Prato M, Guldi DM, Wickstedt JP, Hirsch A. *Nat Mater* 2002;1:190.
- [35] Huang S-CJ, Artyukhin AB, Wang Y, Ju J-W, Stroeve P, Noy A. *J Am Chem Soc* 2005;127:14176.
- [36] Kim JB, Premkumar T, Lee K, Geckeler KE. *Macromol Rapid Commun* 2007;28:276.
- [37] O'Connell MJ, Boul P, Ericson LM, Huffman C, Wang Y, Haroz E, et al. *Chem Phys Lett* 2001;342:265.
- [38] Xu L, Ye Z, Cui Q, Gu Z. *Macromol Chem Phys* 2009;210:2194.
- [39] Baskaran D, Mays JW, Bratcher MS. *Chem Mater* 2005;17:3389.
- [40] Wang D, Chen L. *Nano Lett* 2007;6:1480.
- [41] Liu A, Honma I, Ichihara M, Zhou H. *Nanotechnology* 2006;17:2845.
- [42] Naito M, Nobusawa K, Onouchi H, Nakamura M, Yasui K-I, Ikeda A, et al. *J Am Chem Soc* 2008;130:16697.
- [43] Meyer F, Minoia A, Raquez JM, Spasova M, Lazzaronia R, Dubois P. *J Mater Chem* 2010;20:6873.
- [44] Dong Z, Ye Z. *Polym Chem* 2012;3:286.
- [45] Ye Z, Xu L, Dong Z, Xiang P. *Chem Commun* 2013;49:6235.
- [46] Petrie K, Docoslis A, Vasic S, Kontopoulou M, Morgan S, Ye Z. *Carbon* 2011;49:3378.
- [47] Oaszuwa O, Petrie K, Kontopoulou M, Xiang P, Ye Z, Docoslis A. *Compos Sci Tech* 2012;73:27.
- [48] Xu L, McGraw J-W, Gao F, Grundy M, Ye Z, Gu Z, et al. *J Phys Chem C* 2013;117:10730.
- [49] Johnson LK, Killian CM, Brookhart M. *J Am Chem Soc* 1995;117:6414.
- [50] Ye Z, Zhu S. *Macromolecules* 2003;36:2194.
- [51] Xu Y, Xiang P, Ye Z, Wang W-J. *Macromolecules* 2010;43:8026.
- [52] Ausman KD, Piner R, Lourie O, Ruoff RS, Korobov M. *J Phys Chem B* 2000;104:8911.
- [53] Bahr JL, Mickelson ET, Bronikowski MJ, Smalley RE, Tour JM. *Chem Commun* 2001;193.
- [54] Furtado CA, Kim UJ, Gutierrez HR, Pan L, Dickey EC, Eklund PC. *J Am Chem Soc* 2004;126:6095.
- [55] Landi BJ, Ruf HJ, Worman JJ, Raffaele RP. *J Phys Chem B* 2004;108:17089.
- [56] Maeda Y, Kimura S, Hirashima Y, Kanda M, Lian YF, Wakahara T, et al. *J Phys Chem B* 2004;108:18395.
- [57] Umek P, Vrbancic D, Remskar M, Mertelj T, Venturini P, Pejovnik S, et al. *Carbon* 2002;40:2581.
- [58] Bergin SD, Nicolosi V, Streich PV, Giordani S, Sun Z, Windle AH, et al. *Adv Mater* 1876;2008:20.
- [59] Bergin SD, Sun Z, Rickard D, Streich PV, Hamilton JP, Coleman JN. *ACS Nano* 2009;3:2340.
- [60] May P, Khan U, Hughes JM, Coleman JN. *J Phys Chem C* 2012;116:11393.
- [61] Li CY, Li L, Cai W, Kodjie SL, Tenneti KK. *Adv Mater* 2005;17:1198.
- [62] Li L, Li CY, Ni C. *J Am Chem Soc* 2006;128:1692.
- [63] Laird ED, Li CY. *Macromolecules* 2013;46:2877.